Article

The dental proteome of *Homo antecessor*

https://doi.org/10.1038/s41586-020-2153-8

Received: 4 July 2019

Accepted: 21 January 2020

Published online: 1 April 2020

Check for updates

Frido Welker[1,22]✉, Jazmín Ramos-Madrigal[1,22], Petra Gutenbrunner[2,22], Meaghan Mackie[1,3], Shivani Tiwary[2], Rosa Rakownikow Jersie-Christensen[3], Cristina Chiva[4,5], Marc R. Dickinson[6], Martin Kuhlwilm[7], Marc de Manuel[7], Pere Gelabert[7], María Martinón-Torres[8,9], Ann Margvelashvili[10], Juan Luis Arsuaga[11,12], Eudald Carbonell[13,14], Tomas Marques-Bonet[4,7,15,16], Kirsty Penkman[6], Eduard Sabidó[4,5], Jürgen Cox[2], Jesper V. Olsen[3], David Lordkipanidze[10,17], Fernando Racimo[18], Carles Lalueza-Fox[7], José María Bermúdez de Castro[8,9]✉, Eske Willerslev[18,19,20,21]✉ & Enrico Cappellini[1]✉

The phylogenetic relationships between hominins of the Early Pleistocene epoch in Eurasia, such as *Homo antecessor*, and hominins that appear later in the fossil record during the Middle Pleistocene epoch, such as *Homo sapiens*, are highly debated[1–5]. For the oldest remains, the molecular study of these relationships is hindered by the degradation of ancient DNA. However, recent research has demonstrated that the analysis of ancient proteins can address this challenge[6–8]. Here we present the dental enamel proteomes of *H. antecessor* from Atapuerca (Spain)[9,10] and *Homo erectus* from Dmanisi (Georgia)[1], two key fossil assemblages that have a central role in models of Pleistocene hominin morphology, dispersal and divergence. We provide evidence that *H. antecessor* is a close sister lineage to subsequent Middle and Late Pleistocene hominins, including modern humans, Neanderthals and Denisovans. This placement implies that the modern-like face of *H. antecessor*—that is, similar to that of modern humans—may have a considerably deep ancestry in the genus *Homo*, and that the cranial morphology of Neanderthals represents a derived form. By recovering AMELY-specific peptide sequences, we also conclude that the *H. antecessor* molar fragment from Atapuerca that we analysed belonged to a male individual. Finally, these *H. antecessor* and *H. erectus* fossils preserve evidence of enamel proteome phosphorylation and proteolytic digestion that occurred in vivo during tooth formation. Our results provide important insights into the evolutionary relationships between *H. antecessor* and other hominin groups, and pave the way for future studies using enamel proteomes to investigate hominin biology across the existence of the genus *Homo*.

Since 1994, over 170 human fossil remains have been recovered from level TD6 of the Gran Dolina site of the Sierra de Atapuerca[10] (Burgos, Spain) (Extended Data Fig. 1, Supplementary Information). These fossils have been dated to the late Early Pleistocene epoch and exhibit a unique combination of cranial, mandibular and dental features[9,11]. To accommodate the variation observed in the human fossils from TD6, a new species of the genus *Homo*—*H. antecessor*—was proposed in 1997[9]. The relationship of this species to earlier or later hominins in Eurasia—such as the *H. erectus* specimens from Dmanisi or Neanderthals, Denisovans and modern humans, respectively—have been the subject of considerable debate[3,4,12,13]. These issues remain unresolved owing to the fragmentary nature of hominin fossils at other sites, and the failure to recover ancient DNA in Eurasia that dates to the Early, and most of the Middle, Pleistocene epoch.

By contrast, recent developments in the extraction and tandem mass-spectrometric analysis of ancient proteins have made it possible to retrieve phylogenetically informative protein sequences from Early Pleistocene contexts[6,8]. We therefore applied ancient protein analysis to a *H. antecessor* molar from sublevel TD6.2 of the Gran Dolina site of the Sierra de Atapuerca (specimen ATD6-92) (Extended Data Fig. 2a). This specimen, identified as an enamel fragment of a permanent lower left first or second molar, has been directly dated to 772–949 thousand

[1]Evolutionary Genomics Section, Globe Institute, University of Copenhagen, Copenhagen, Denmark. [2]Computational Systems Biochemistry, Max Planck Institute of Biochemistry, Martinsried, Germany. [3]The Novo Nordisk Foundation Center for Protein Research, University of Copenhagen, Copenhagen, Denmark. [4]Center for Genomic Regulation (CNAG-CRG), Barcelona Institute of Science and Technology, Barcelona, Spain. [5]Proteomics Unit, University Pompeu Fabra, Barcelona, Spain. [6]Department of Chemistry, University of York, York, UK. [7]Institute of Evolutionary Biology (UPF-CSIC), University Pompeu Fabra, Barcelona, Spain. [8]Centro Nacional de Investigación sobre la Evolución Humana (CENIEH), Burgos, Spain. [9]Anthropology Department, University College London, London, UK. [10]Georgian National Museum, Tbilisi, Georgia. [11]Centro Mixto UCM-ISCIII de Evolución y Comportamiento Humanos, Madrid, Spain. [12]Departamento de Paleontología, Facultad de Ciencias Geológicas, Universidad Complutense de Madrid, Madrid, Spain. [13]Departamento d'Història i Història de l'Art, Universidad Rovira i Virgili, Tarragona, Spain. [14]Institut Català de Paleoecologia Humana i Evolució Social (IPHES), Tarragona, Spain. [15]Catalan Institution of Research and Advanced Studies (ICREA), Barcelona, Spain. [16]Institut Català de Paleontologia Miquel Crusafont, Universitat Autònoma de Barcelona, Barcelona, Spain. [17]Tbilisi State University, Tbilisi, Georgia. [18]Lundbeck Foundation GeoGenetics Centre, Globe Institute, University of Copenhagen, Copenhagen, Denmark. [19]Department of Zoology, University of Cambridge, Cambridge, UK. [20]Wellcome Sanger Institute, Hinxton, UK. [21]Danish Institute for Advanced Study, University of Southern Denmark, Odense, Denmark. [22]These authors contributed equally: Frido Welker, Jazmín Ramos-Madrigal, Petra Gutenbrunner.
✉e-mail: frido.welker@sund.ku.dk; josemaria.bermudezdecastro@cenieh.es; ewillerslev@sund.ku.dk; ecappellini@sund.ku.dk

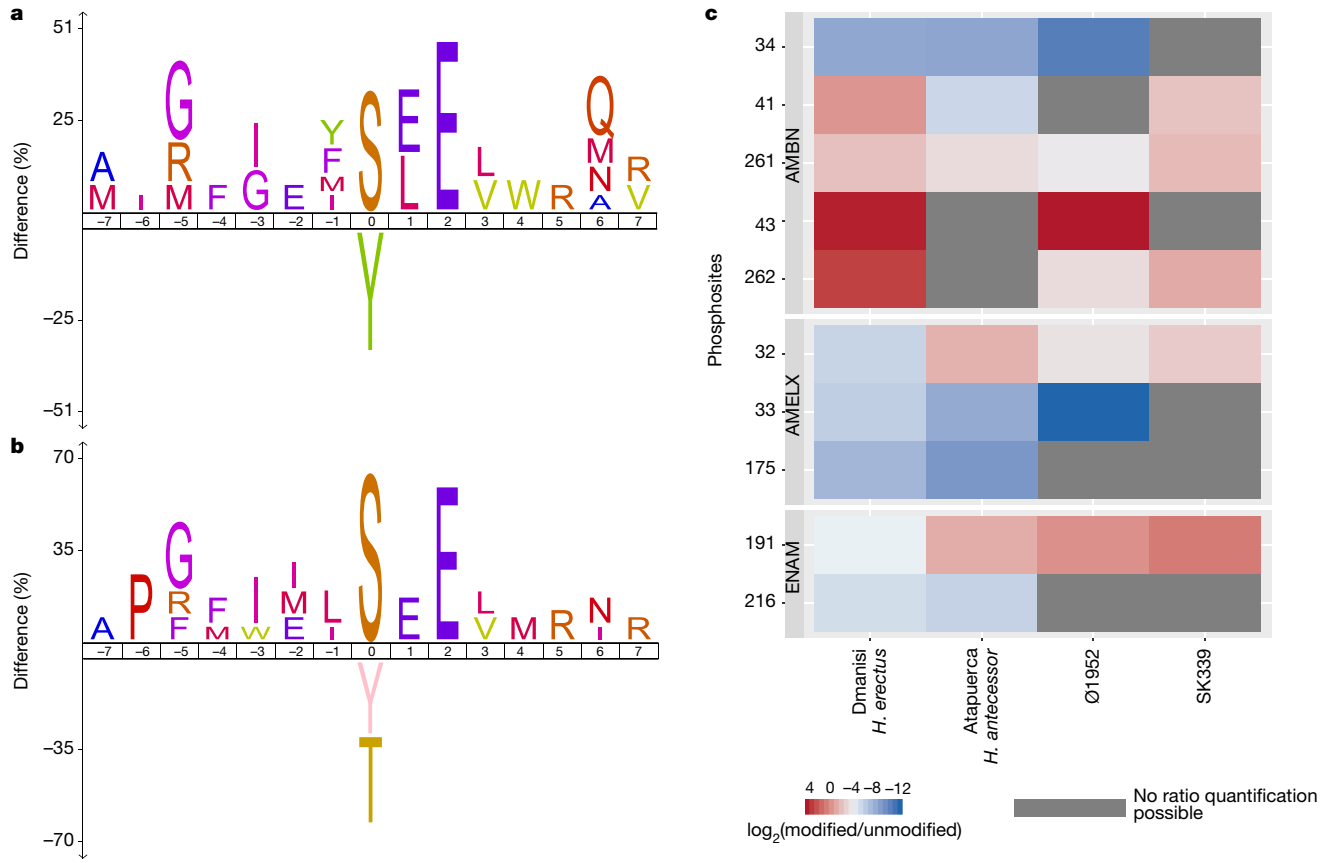

Fig. 1 | Phosphorylation of hominin enamel proteomes. a, Phosphorylation sequence motif analysis of *H. antecessor* specimen ATD6-92. **b**, Phosphorylation sequence motif analysis of *H. erectus* specimen D4163. **c**, Phosphorylation occupancy comparison, expressed as $\log_2$-transformed summed intensity ratio of modified and unmodified peptides, for amino acid sites for which data are available for at least two specimens. *y* axis labels indicate the position of the phosphorylated amino acids for each protein (UniProt accession numbers Q9NP70 (AMBN), Q99217 (AMELX) and Q9NRM1 (ENAM)). SK339 denotes an archaeological specimen from a modern human, which is approximately three centuries old (see 'Recent human control specimens' in the Methods for details).

years ago (ka) using a combination of electron spin resonance and U-series dating[11]. In addition, we sampled dentine and enamel from an isolated *H. erectus* upper first molar (specimen D4163) (Extended Data Fig. 2b) from Dmanisi (Georgia) that has been dated to 1.77 million years ago (Ma)[1,14,15], as amino acid racemization analysis of this specimen indicated the presence of an endogenous protein component in the intracrystalline enamel fraction of the tooth (Extended Data Fig. 3, Supplementary Information). On both specimens, we performed digestion-free peptide extraction optimized for the recovery of short, degraded protein remains[6]. Nanoscale liquid chromatography–tandem mass spectrometry (nanoLC–MS/MS) acquisition was replicated in two independent proteomic laboratories (Extended Data Table 1), implementing common precautions and analytical workflows to minimize protein contamination (Methods). We compared the proteomic datasets retrieved from the Pleistocene hominin tooth specimens with those generated from a positive control, a recent human premolar (Ø1952; which is from a male individual and is approximately three centuries old), as well as previously published Holocene teeth[16] (Methods, Supplementary Information). Finally, to validate our enamel peptide spectrum matches, we performed machine-learning-based MS/MS spectrum intensity prediction using the wiNNer algorithm[17]. The results show that the wiNNer model retrained for randomly cleaved and heavily modified peptides provides a predictive performance similar to that of the wiNNer model trained on modern, trypsin-digested samples, assuring accurate sequence identification for the phylogenetically informative peptides (median Pearson correlation coefficients of ≥0.76) (Methods, Supplementary Fig. 6, Supplementary Information).

Protein recovery from the Dmanisi dentine sample was limited to sporadic collagen type I fragments, and therefore in-depth analysis of this material was not further pursued. By contrast, we recovered ancient proteomes from both hominin enamel samples. We found that the composition of these proteomes is similar to that of the recent human specimen that we processed as a positive control, as well as to previously published proteomes from ancient enamel[6,16,18,19] (Extended Data Table 2, Supplementary Table 6). The enamel-specific proteins include amelogenin (both AMELX and AMELY isoforms), enamelin (ENAM), ameloblastin (AMBN), amelotin (AMTN) and the enamel-specific protease matrix metalloproteinase 20 (MMP20). Serum albumin (ALB) and collagens (COL1α1, COL1α2 and COL17α1) are also present. For the enamel-specific proteins, the peptide sequences that we retrieved cover approximately the same protein regions in all of the specimens that we analysed (Extended Data Fig. 4). Although destructive, our sampling of Pleistocene hominin teeth resulted in higher protein sequence coverage than acid-etching of Holocene enamel surfaces[16,20] (Supplementary Fig. 7). The AMTN-specific peptides largely derive from a single sequence region involved in hydroxyapatite precipitation through the presence of phosphorylated serines[21]. Finally, the observation of the AMELY-specific peptides (which is coded on the non-recombinant portion of the Y chromosome) demonstrates that the *H. antecessor* molar that we studied belonged to a male individual[16] (Extended Data Fig. 5).

Besides proteome composition and sequence coverage, several further lines of evidence independently support the endogenous origin of the hominin enamel proteomes. Unlike exogenous trypsin, keratins and other human-skin contaminants that we identified, the enamel

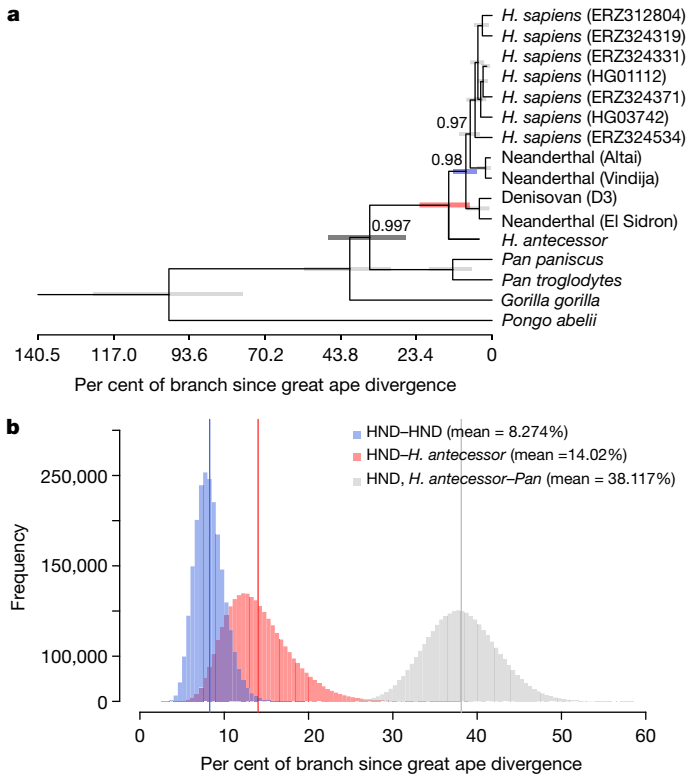

Fig. 2 | Phylogenetic analysis of *H. antecessor* ATD6-92. a, Maximum credibility tree estimated using BEAST and a concatenated alignment of seven protein sequences recovered for the ancient sample. Posterior Bayesian probabilities are indicated at nodes with a probability of ≤ 1. Horizontal error bars at each node indicate the 95% highest posterior density intervals for the split time estimates. The position of *H. antecessor* is consistent with that obtained via maximum likelihood (Supplementary Fig. 13) and Bayesian (Supplementary Fig. 16) analyses. ERZ and HG codes in parentheses after *H. sapiens* refer to identifiers for data from the Simons Genome Diversity Panel[33] and 1000 Genomes Project[34], respectively (see 'Comparison between the ancient protein sequences and modern reference proteins' in the Methods for details). **b**, Histograms of the divergence times obtained for the split between *H. antecessor* and the *H. sapiens*, Neanderthal and Denisovan clade (HND) (red), the HND–HND split (blue), and the *Pan*–(HND + *H. antecessor*) split (grey). Divergence times in **a** and **b** are shown as a percentage of the time since the divergence of all great apes.

proteins have high deamidation rates (Extended Data Fig. 6)—above the rate observed for the recent human specimens (Supplementary Fig. 8). Both Pleistocene hominins have average peptide lengths that are shorter than those observed for our recent human controls (Extended Data Fig. 6d). The average peptide length is shorter in the Dmanisi hominin, but longer in the younger Atapuerca hominin (Extended Data Fig. 6d). By contrast, we observe that the peptide lengths in enamel from the Dmanisi hominin are indistinguishable from those of the faunal remains from the same site. Together, our protein data are therefore consistent with theoretical and experimental[6,22] expectations for samples of their relative age.

In addition to diagenetic modifications, we observe two kinds of in vivo modification in our recent and ancient enamel proteomes. First, we detect serine (S) phosphorylation within the S-X-E motif (Fig. 1a, b). This motif, as well as the S-X-phosphorylated S motif, is recognized by the FAM20C secreted kinase, which is active in the phosphorylation of extracellular proteins[23,24]. The presence of phosphoserine in fossil enamel and its location in the S-X-E and/or S-X-phosphorylated S motifs has also previously been observed in other Pleistocene enamel proteomes[6,25]. Phosphorylation occupancy can be computed successfully for ancient and recent samples, and reveals differences in the ratios of phosphorylated peptides between samples (Fig. 1c, Supplementary Table 5). Second, the peptide populations that we retrieve primarily cover the ameloblastin, enamelin and amelogenin sequence regions, representing cleavage products deriving from in vivo activity of the proteases MMP20 and—subsequently—kallikrein 4 (KLK4) (Extended Data Fig. 4, Methods). The peptide populations are also enriched in N and C termini that correspond to known MMP20 and KLK4 cleavage sites (Extended Data Fig. 7, Supplementary Fig. 9). FAM20C phosphorylation and MMP20 and KLK4 proteolysis are the two main processes that occur in vivo during enamel biomineralization. Our observation of products deriving from both processes opens up the possibility of studying in vivo processes of hominin tooth formation across the Pleistocene epoch.

Homo antecessor is known only from the Gran Dolina TD6 assemblage in Atapuerca[9]. Its relationship with other European Middle Pleistocene fossils is heavily debated[3–5,26,27]. It remains contentious as to whether *H. antecessor* represents the last common ancestor of *H. sapiens*, Neanderthals and Denisovans[9], or whether it represents a sister lineage to the last common ancestor of these species[28,29]. We address this issue by conducting phylogenetic analyses on the basis of our ancient protein sequences from *H. antecessor* (ATD6-92), a panel of present-day great ape genomes and protein sequences translated from archaic hominin genomes (Methods).

We built several phylogenetic trees using maximum likelihood and Bayesian methods (Fig. 2a, Supplementary Figs. 13–16). In these trees, the *H. antecessor* sequence represents a sister taxon that is closely related to, but not part of, the group composed of Late Pleistocene hominins for which molecular data are available (Fig. 2a, Supplementary Figs. 13, 15, 16). The enamel protein sequences do not resolve the relationships between *H. sapiens*, Neanderthals and Denisovans owing to the low number of informative single amino acid polymorphisms. However, pairwise divergence of the amino acid sequences between *H. antecessor* and the clade containing *H. sapiens*, Neanderthals and the Denisovan is larger than the divergence between the members of this clade (Fig. 2b, Supplementary Fig. 12, Supplementary Information). The concatenated gene tree may be subjected to incomplete lineage sorting, and we have too little sequence data to discard this possibility at the moment. However, if we use the concatenation of available gene trees as a best guess for the population tree, and assume that such a population tree is a good descriptor of the relationships among ancient hominins, then our results support the placement of *H. antecessor* as a closely related sister taxon of the last common ancestor of *H. sapiens*, Neanderthals and Denisovans. The phylogenetic position of *H. antecessor* agrees with a divergence of the *H. sapiens* and Neanderthal + Denisovan lineages between 550 and 765 ka[30,31], as ATD6-92 has been dated to 772–949 ka[11]. This is further supported by recent reconsiderations of the morphology of *H. antecessor* in relation to Middle and Late Pleistocene hominins[29].

Homo antecessor has tentatively been proposed as the last common ancestor of Neanderthals and modern humans[9]. The similarities observed between the modern-like mid-facial topography of *H. antecessor* and *H. sapiens*—including a modern pattern of coronal orientation of the infraorbital surface, the sloping and directionality of this plane, as well as the anterior flexion of the maxillary surface and arching of the zygomatic-alveolar crest—were key in this proposal[9,32]. Additional studies of the face of ATD6-69 have confirmed that *H. antecessor* exhibits the oldest known modern-like face in the fossil record[12,13]. The phylogenetic placement of *H. antecessor* implies that this modern-like face—as represented by *H. antecessor*—must have a considerably deep ancestry in the genus *Homo*. Findings made between 2003 and 2005 have shown that the *H. antecessor* hypodigm includes some features that were previously considered Neanderthal autapomorphies[28]. Our results suggest that these features appeared in Early Pleistocene hominins, and were retained by Neanderthals and lost by modern humans.

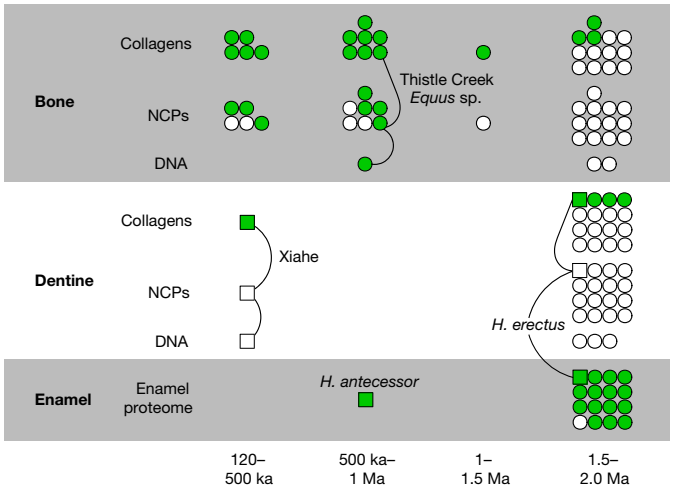

Fig. 3 | Skeletal proteome preservation in the Middle and Early Pleistocene epoch (0.12–2.6 Ma). For each sample, the presence (green) or absence (blank) of endogenous DNA, collagens, non-collagenous proteins (NCPs) or an enamel proteome is given. Only samples for which mammalian proteomes are published are considered[6–8,35–38]. Hominin samples are indicated with squares, other mammalian samples are indicated with circles. Selected specimens have their separate molecular components joined, and are named. Xiahe refers to the Xiahe mandible[7]; the Thistle Creek *Equus* refers to a horse metapodial from the Canadian permafrost[38].

By contrast, the phylogenetic tree built with the *H. erectus* specimen from Dmanisi has only moderate resolution (Extended Data Fig. 8, Supplementary Fig. 11), despite deeper shotgun protein sequencing for this specimen (Extended Data Table 1). This partly inconclusive result might be due to the shorter average peptide lengths compared to the Atapuerca *H. antecessor* specimen (Extended Data Fig. 6d, Methods) and an absence of uniquely segregating single amino acid polymorphisms (Supplementary Table 9). Although our *H. erectus* data from Dmanisi demonstrate that ancient hominin proteins can be reliably obtained from the Early Pleistocene epoch, they also highlight the current limits of ancient protein analysis when applied to the phylogenetic placement of Early Pleistocene hominin remains.

Our dataset provides a unique molecular resource of hominin biomolecular sequences from Early and Middle Pleistocene hominins, and represents—to our knowledge—the oldest ancient hominin proteomes presented to date. Comparison of hominin and fauna proteomes from different skeletal tissues reveals that the dental enamel proteome outlasts dentine and bone proteome preservation (Fig. 3). Here the prolonged survival of hominin enamel proteomes is exploited to show that *H. antecessor* represents a hominin taxon closely related to the last common ancestor of *H. sapiens*, Neanderthals and Denisovans. In addition, our datasets demonstrate that in vivo proteome modifications, such as serine phosphorylation, survive over time scales of hundreds of thousands of years. Current research therefore suggests that dental enamel, the hardest tissue in the mammalian skeleton, is the material of choice for the analysis of hominin evolution in deep time.

Online content

Any methods, additional references, Nature Research reporting summaries, source data, extended data, supplementary information, acknowledgements, peer review information; details of author contributions and competing interests; and statements of data and code availability are available at https://doi.org/10.1038/s41586-020-2153-8.

1. Gabunia, L. et al. Earliest Pleistocene hominid cranial remains from Dmanisi, Republic of Georgia: taxonomy, geological setting, and age. *Science* **288**, 1019–1025 (2000).
2. Zhu, Z. et al. Hominin occupation of the Chinese Loess Plateau since about 2.1 million years ago. *Nature* **559**, 608–612 (2018).
3. Stringer, C. The origin and evolution of *Homo sapiens*. *Phil. Trans. R. Soc. Lond. B* **371**, 20150237 (2016).
4. Hublin, J. J. The origin of Neandertals. *Proc. Natl Acad. Sci. USA* **106**, 16022–16027 (2009).
5. Rightmire, G. Human evolution in the Middle Pleistocene: the role of *Homo heidelbergensis*. *Evol. Anthropol.* **6**, 218–227 (1998).
6. Cappellini, E. et al. Early Pleistocene enamel proteome from Dmanisi resolves *Stephanorhinus* phylogeny. *Nature* **574**, 103–107 (2019).
7. Chen, F. et al. A late Middle Pleistocene Denisovan mandible from the Tibetan Plateau. *Nature* **569**, 409–412 (2019).
8. Welker, F. et al. Enamel proteome shows that *Gigantopithecus* was an early diverging pongine. *Nature* **576**, 262–265 (2019).
9. Bermúdez de Castro, J. M. et al. A hominid from the lower Pleistocene of Atapuerca, Spain: possible ancestor to Neandertals and modern humans. *Science* **276**, 1392–1395 (1997).
10. Carbonell, E. et al. Lower Pleistocene hominids and artifacts from Atapuerca-TD6 (Spain). *Science* **269**, 826–830 (1995).
11. Duval, M. et al. The first direct ESR dating of a hominin tooth from Atapuerca Gran Dolina TD-6 (Spain) supports the antiquity of *Homo antecessor*. *Quat. Geochronol.* **47**, 120–137 (2018).
12. Freidline, S. E., Gunz, P., Harvati, K. & Hublin, J.-J. Evaluating developmental shape changes in *Homo antecessor* subadult facial morphology. *J. Hum. Evol.* **65**, 404–423 (2013).
13. Lacruz, R. S. et al. Facial morphogenesis of the earliest Europeans. *PLoS One* **8**, e65199 (2013).
14. Ferring, R. et al. Earliest human occupations at Dmanisi (Georgian Caucasus) dated to 1.85–1.78 Ma. *Proc. Natl Acad. Sci. USA* **108**, 10432–10436 (2011).
15. Lordkipanidze, D. et al. A complete skull from Dmanisi, Georgia, and the evolutionary biology of early *Homo*. *Science* **342**, 326–331 (2013).
16. Stewart, N. A., Gerlach, R. F., Gowland, R. L., Gron, K. J. & Montgomery, J. Sex determination of human remains from peptides in tooth enamel. *Proc. Natl Acad. Sci. USA* **114**, 13649–13654 (2017).
17. Tiwary, S. et al. High-quality MS/MS spectrum prediction for data-dependent and data-independent acquisition data analysis. *Nat. Methods* **16**, 519–525 (2019).
18. Castiblanco, G. A. et al. Identification of proteins from human permanent erupted enamel. *Eur. J. Oral Sci.* **123**, 390–395 (2015).
19. Asaka, T. et al. Type XVII collagen is a key player in tooth enamel formation. *Am. J. Pathol.* **174**, 91–100 (2009).
20. Porto, I. M., Laure, H. J., de Sousa, F. B., Rosa, J. C. & Gerlach, R. F. New techniques for the recovery of small amounts of mature enamel proteins. *J. Archaeol. Sci.* **38**, 3596–3604 (2011).
21. Gasse, B., Chiari, Y., Silvent, J., Davit-Béal, T. & Sire, J.-Y. Amelotin: an enamel matrix protein that experienced distinct evolutionary histories in amphibians, sauropsids and mammals. *BMC Evol. Biol.* **15**, 47 (2015).
22. Demarchi, B. et al. Protein sequences bound to mineral surfaces persist into deep time. *eLife* **5**, e17092 (2016).
23. Tagliabracci, V. S. et al. Secreted kinase phosphorylates extracellular proteins that regulate biomineralization. *Science* **336**, 1150–1153 (2012).
24. Hu, J. C. C., Yamakoshi, Y., Yamakoshi, F., Krebsbach, P. H. & Simmer, J. P. Proteomics and genetics of dental enamel. *Cells Tissues Organs* **181**, 219–231 (2005).
25. Glimcher, M. J., Cohen-Solal, L., Kossiva, D. & de Ricqles, A. Biochemical analyses of fossil enamel and dentin. *Paleobiology* **16**, 219–232 (1990).
26. Wagner, G. A. et al. Radiometric dating of the type-site for *Homo heidelbergensis* at Mauer, Germany. *Proc. Natl Acad. Sci. USA* **107**, 19726–19730 (2010).
27. Martinón-Torres, M. et al. Dental evidence on the hominin dispersals during the Pleistocene. *Proc. Natl Acad. Sci. USA* **104**, 13279–13282 (2007).
28. Bermúdez de Castro, J. M., Martinón-Torres, M., Arsuaga, J. L. & Carbonell, E. Twentieth anniversary of *Homo antecessor* (1997–2017): a review. *Evol. Anthropol.* **26**, 157–171 (2017).
29. Gómez-Robles, A., Bermúdez de Castro, J. M., Arsuaga, J.-L., Carbonell, E. & Polly, P. D. No known hominin species matches the expected dental morphology of the last common ancestor of Neanderthals and modern humans. *Proc. Natl Acad. Sci. USA* **110**, 18196–18201 (2013).
30. Meyer, M. et al. Nuclear DNA sequences from the Middle Pleistocene Sima de los Huesos hominins. *Nature* **531**, 504–507 (2016).
31. Prüfer, K. et al. The complete genome sequence of a Neanderthal from the Altai Mountains. *Nature* **505**, 43–49 (2014).
32. Lacruz, R. S. et al. The evolutionary history of the human face. *Nat. Ecol. Evol.* **3**, 726–736 (2019).
33. Mallick, S. et al. The Simons Genome Diversity Project: 300 genomes from 142 diverse populations. *Nature* **538**, 201–206 (2016).
34. The 1000 Genomes Project Consortium. A global reference for human genetic variation. *Nature* **526**, 68–74 (2015).
35. Welker, F. et al. Middle Pleistocene protein sequences from the rhinoceros genus *Stephanorhinus* and the phylogeny of extant and extinct Middle/Late Pleistocene Rhinocerotidae. *PeerJ* **5**, e3033 (2017).
36. Hill, R. C. et al. Preserved proteins from extinct *Bison latifrons* identified by tandem mass spectrometry; hydroxylysine glycosides are a common feature of ancient collagen. *Mol. Cell. Proteomics* **14**, 1946–1958 (2015).
37. Wadsworth, C. & Buckley, M. Proteome degradation in fossils: investigating the longevity of protein survival in ancient bone. *Rapid Commun. Mass Spectrom.* **28**, 605–615 (2014).
38. Orlando, L. et al. Recalibrating *Equus* evolution using the genome sequence of an early Middle Pleistocene horse. *Nature* **499**, 74–78 (2013).

Methods

No statistical methods were used to predetermine sample size. The experiments were not randomized and investigators were not blinded to allocation during experiments and outcome assessment.

Site location and specimen selection

Recent human control specimens. We analysed Ø1952, a human premolar recovered in an archaeological excavation in Copenhagen (Almindeligt Hospital Kirkegård, excavated in 1952, from kisse '2'). The tooth is approximately three centuries old, as the cemetery was in use from approximately AD 1600 to approximately AD 1800, and originates from a male individual. We also re-analysed previously published data[16] related to specimens that are dated to between approximately 5,700 and 200 years ago; of these specimens, we took SK339 as a recent example in our comparative figures (a male individual from Fewston (UK) dated to the nineteenth century AD).

Atapuerca. One fragmentary permanent lower left first or second molar (ATD6-92; field number and museum accession number at CENIEH) was used for ancient protein analysis (Extended Data Fig. 2a, Supplementary Information). ATD6-92 originates from sublevel TD6.2 of the Gran Dolina cave site. Sublevel TD6.2 contains a large number of faunal remains, about 170 hominin fossils and about 830 archaeological artefacts. All hominin specimens from sublevel TD6.2, including ATD6-92, are attributed to *H. antecessor*[9]. ATD6-92 has recently been directly dated through electron spin resonance, laser-ablation inductively coupled plasma mass spectrometry U-series and bulk U-series dating[11]. Together with previous chronological research at the site, these analyses constrain the age of ATD6-92 to 772–949 thousand years old[11].

Dmanisi. One fragmentary permanent upper first molar (D4163; field number and museum accession number at the Georgian National Museum) was used for ancient protein analysis (Extended Data Fig. 2b, Supplementary Information). D4163 derives from layer B1 in excavation block M6 (Dmanisi). Layer B1 at Dmanisi contains one of the richest palaeontological assemblages attributed to the Eurasian Early Pleistocene epoch, including several hominin crania. Below, we refer to these specimens as *H. erectus* (Dmanisi). They represent the earliest hominin fossils outside Africa, and are dated to 1.77 Ma[14]. Faunal material from the site previously demonstrated ancient protein survival for most specimens, but a total absence of ancient DNA[6] (Fig. 3).

Amino acid racemization

Chiral amino acid analysis was undertaken on one Pleistocene sample from the hominin tooth (D4163) to test the endogeneity of the enamel protein through its degradation patterns. The tooth chip was separated into the enamel and dentine portions, and each was powdered with an agate pestle and mortar. All samples were prepared using previously published procedures[39], modified to be optimized for enamel, using a bleach time of 72 h to isolate the intracrystalline protein, demineralization in HCl, KOH neutralization and formation of a biphasic solution through centrifugation[40]. Two subsamples were analysed from each portion: one fraction was directly demineralized and the free amino acids analysed, and the second was treated to release the peptide-bound amino acids, thus yielding the total hydrolysable amino acid fraction. Samples were analysed in duplicate by reversed-phase high-performance liquid chromatography, with standards and blanks analysed alongside samples. During preparative hydrolysis, both asparagine (Asn) and glutamine (Gln) undergo rapid irreversible deamidation to aspartic acid (Asp) and glutamic acid (Glu), respectively[41]. It is therefore not possible to distinguish between the acidic amino acids and their derivatives, and they are reported together as Asx and Glx, respectively. Additional descriptions of the methods, as well as additional results, are given in the Supplementary Information.

Proteomic extraction and nanoLC–MS/MS

Protein extraction. Protein extraction was conducted on enamel samples (from the Atapuerca *H. antecessor*, Dmanisi *H. erectus* and Ø1952) and a dentine sample (Dmanisi), using one of three protocols. In brief, the first extraction method used HCl for demineralization, but included no subsequent reduction, alkylation or digestion. The second extraction method used a more standard approach, in which the pellet left from the demineralization in extraction one was reduced, alkylated and digested with LysC and trypsin. The third extraction method used TFA for demineralization, and had no subsequent reduction, alkylation or digestion. The first and third extraction approaches provided more extensive peptide recovery in ancient enamel proteomes[6] compared to the second extraction approach[42]. Further details can be found in the Supplementary Information and a previous publication[6]. Ø1952 was processed using extraction methods one and three. No proteinase and phosphatase inhibitors were used during extraction, as we assumed that catalytically active enzymes were not present in our specimens and the high acidic conditions during our extraction would have irreversibly denatured any proteases possibly present as contaminants in our reagents. Extended Data Table 1 provides a breakdown of the use of specific extraction methods, hominin samples and hominin tissues.

NanoLC–MS/MS analysis. Shotgun proteomic data were obtained on peptide extracts of both hominins at separate facilities at the Novo Nordisk Centre for Protein Research (University of Copenhagen) and the Proteomics Unit (Centre for Genomic Regulation, Barcelona Institute of Science and Technology). Full peptide elutions were injected, in some cases across replicate runs in both Copenhagen and Barcelona. In brief, samples processed in Copenhagen were suspended in 0.1% trifluoroacetic acid, 5% acetonitrile, and analysed on a Q-Exactive HF or HF-X mass spectrometer (Thermo Fisher Scientific) coupled to an EASY-nLC 1200 (Thermo Fisher Scientific). The HF or HF-X mass spectrometer was operated in positive ion mode with a nanospray voltage of 2 kV and a source temperature of 275 °C. Data-dependent acquisition mode was used for all mass spectrometric measurements. Full mass spectrometry scans were done at a resolution of 120,000 with a mass range of m/z 300–1,750 and 350–1,400 for the HF and HF-X mass spectrometers, respectively, with detection in the Orbitrap mass analyser. Fragment ion spectra were produced at a resolution of 60,000 via high-energy collision dissociation (HCD) at a normalized collision energy of 28% and acquired in the Orbitrap mass analyser. In addition, test runs for the Dmanisi sample were performed at a shorter gradient (Supplementary Information). In Barcelona, samples were dissolved in 0.1% formic acid and analysed on a LTQ-Orbitrap Fusion Lumos mass spectrometer (Thermo Fisher Scientific) coupled to an EASY-nLC 1000. The mass spectrometer was operated similarly to the parameters stated for the HF and HF-X mass spectrometers in Copenhagen, except the nanospray voltage was 2.4 kV and full mass spectrometry scans with 1 micro scan were used over a mass range of m/z 350–1,500. Further details of the LC–MS/MS analysis can be found in the Supplementary Information.

Proteomic data analysis

Protein sequence database construction. We constructed an initial Hominidae sequence database containing protein sequences of all major and minor enamel proteins derived from all extant great apes, a hylobatid (*Nomascus leucogenys*) and a macaque (*Macaca mulatta*). Additionally, we added protein sequences translated from extinct Late Pleistocene hominins[30,43], and sequences from *Gorilla beringei*, *Pongo pygmaeus* and *Pongo tapanuliensis*[44–46]. For each protein, we reconstructed the protein sequence of ancestral nodes in the Hominidae family through PhyloBot[47] to minimize cross-species proteomic effects[48], and added missing isoform variation on the basis of the isoforms present for each protein in the human proteome as given by UniProt (Supplementary Information). Furthermore, we downloaded

the entire human reference proteome from UniProt (4 September 2018) for a single separate search to allow matches to proteins previously not encountered in enamel proteomes. To each constructed database, we added a set of known or possible laboratory contaminants to allow for the identification of possible protein contaminants[49].

Proteomic software, settings and false-discovery rate. Raw mass spectrometry data were searched for each specimen and tissue separately in either PEAKS[50] (v.7.5) or MaxQuant[51] (v.1.5.3.30). No fixed modifications were specified in any search. For PEAKS, variable post-translational modifications were set to include proline hydroxylation, glutamine and asparagine deamidation, oxidation (M), phosphorylation (STY), carbamidomethylation (C) and pyroglutamic acid (from Q and E). For MaxQuant, the following variable post-translation modifications were additionally included: ornithine formation (R), oxidation (W), dioxidation (MW), histidine to aspartic acid (H>D), and histidine to hydroxyglutamate. Searches were conducted with unspecific digestion. For PEAKS, precursor mass tolerance was set to 10 ppm and fragment mass tolerance to 0.05 Da, and the false-discovery rate of peptide spectrum matches was set to equal ≤1.0%. For MaxQuant, default settings of 20 ppm for the first search and 4.5 ppm for the final search were used, a fragment mass tolerance of 20 ppm, and peptide spectrum match (PSM) and protein false-discovery rate was set to 1.0%, with a minimum required Andromeda score of 40 for all peptides. Protein matches were accepted with a minimum of two unique peptide matches in either the PEAKS or MaxQuant search. Proteins that conform to these criteria are detailed in Extended Data Table 2. Example MS/MS spectra from the MaxQuant search and overlapping sites of phylogenetic interest (single amino acid polymorphisms) are included as Supplementary Data 1.

Data search iterations. For both the proteomes of Dmanisi and Atapuerca specimens, we conducted two separate initial searches. First, we conducted a search in PEAKS against the entire human proteome. Only standard enamel proteins were identified in these searches, allowing us to continue with more specific searches. For the Dmanisi dentine sample, this first search resulted in a small number of peptides matching to collagen type I only. On the basis of the limited amount of sequence data, no further analysis of the Dmanisi dentine data was therefore conducted. Second, for the enamel data, we conducted a search in PEAKS and MaxQuant against the entire enamel proteome database of all extant and extinct Hominidae. This search was used to observe single amino acid polymorphisms outside the known sequence variation in PEAKS and MaxQuant through the de novo, error-tolerant and/or dependent peptide approaches implemented in each of these search engines. These initial searches indicate overall good protein preservation in both samples and the presence of peptide matches to *Pan*- and *Homo*-derived proteins only.

On the basis of these two initial searches, a novel protein sequence database was used that only includes sequences from the genus *Pan*, the genus *Homo*, their predicted ancestral sequences and novel protein sequences observed for both the Dmanisi or Atapuerca samples. Final searches and subsequent data analysis were conducted against this database using the above search and post-translational modification settings. Positions supported by insufficient spectral data were replaced by 'X', in resulting peptide alignments before phylogenetic analysis.

Data analysis of Ø1952 and the previously published[16] dataset was conducted only in MaxQuant against a database restricted to *H. sapiens*. All other search settings and database restrictions were similar between these two recent human controls and the ancient hominin proteomes.

Peptide sequence and single amino acid polymorphism validation. To validate the PSMs covering single amino acid polymorphisms of interest, we performed peptide spectrum intensity prediction and validation on our dataset using wiNNer[17]. Data from the ancient specimens (Dmanisi *H. erectus* and Atapuerca *H. antecessor*) were divided into a subset that contained phylogenetically informative peptide sequences and a larger subset that did not contained these peptides. A training dataset was prepared by taking a subset of the latter peptides, and adding a previously published dataset of enamel proteomes from Dmanisi fauna[6]. We built two models, one for HCD +2 spectra and one for HCD +3 spectra. We took into account the large number of variable modifications observed in our ancient enamel proteomes, and split the retained data for each model into subsets for training, validation and testing (80:10:10). We then obtained Pearson correlation coefficients for the predicted and true fragment intensities in the test dataset and the phylogenetically informative spectra. The architecture of wiNNer was built using Keras (version 2.0.8; https://keras.io) and Tensorflow (version 1.3.0). The wiNNer analysis indicated close correspondence between predicted and true fragment ion intensities (Pearson correlation coefficient medians between 0.85 and 0.76 for different subsets of the data), indicating adequate peptide sequence identification for all our peptides, including phylogenetically informative positions and the variable post-translational modifications. The wiNNer model can be accessed on GitHub (https://github.com/cox-labs/wiNNer.git). Additional methodological details of the wiNNer architecture are given in the Supplementary Information.

Protein damage analysis. Ancient proteins can be modified diagenetically in a variety of ways compared to their modern counterparts. We quantify glutamine and asparagine deamidation following a previously publication[42] for MaxQuant output, based on MS1 spectral intensities and protein-based bootstrapping (1,000 bootstraps). Further details can be found in the previous publication[42]. We observe that both glutamines and asparagines are almost all deamidated to glutamic acid and aspartic acid, respectively (Extended Data Fig. 6a–c). In addition, peptide length distributions were obtained for datasets presented here and elsewhere[6,8], demonstrating a shortening of average peptide length and overall peptide length distributions for older samples (Extended Data Fig. 6d).

Protein in vivo modification analysis. The existing literature on enamel and enamel proteome biomineralization describes three processes that are key to the maturation of the enamel proteome: protein hydrolysis by MMP20 and KLK4[52–55], in vivo phosphorylation of serine residues[6,8,23] and expression of different isoforms of AMELX, AMBN and AMTN[52,55,56]. We sought to explore the presence of both in vivo protein hydrolysis and serine phosphorylation modifications in our Pleistocene hominin proteomes.

For protein hydrolysis by MMP20 and KLK4, we made use of the Atapuerca digestion-free dataset and the described locations of AMBN, AMELX and AMELY, and ENAM cleavage by MMP20 and KLK4[52–55]. We compared the experimentally observed cleavage sites to a random cleavage model of each protein separately and tested whether the cleavage sites are present in a larger portion of PSMs in the ancient sample. Here we can indeed show an increased presence of PSMs with termini at, or close to, known MMP20 and KLK4 cleavage locations (Extended Data Fig. 7). This corresponds with our observation that protein regions with continuous sequence coverage correspond to known proteolytic fragments after MMP20 and KLK4 activity (Extended Data Fig. 4).

Phosphorylation of serines (S), threonines (T) and tyrosines (Y) was assessed using Icelogo[57] sequence motif analysis. This analysis was based on the MaxQuant results, from which only identified phosphorylation sites with a localization probability of ≥0.95 were selected. STY sites with no phosphorylation or localization probabilities ≤ 0.95 were taken as the non-phosphorylated background, and a sequence motif window of 7 amino acids on either side of the STY was selected. Sequence motif analysis indicates a strong preference for the phosphorylation of S with a glutamic acid (E) on the +2 position (S-X-E motif) (Fig. 1a, b) in both hominin enamel proteomes. This substrate motif

and the S-X-phosphorylated S motif are recognized by the kinase FAM20C, which is known to be active in vivo on extracellular proteins involved in biomineralization[23], and has previously been reported for ancient, non-hominin enamel proteomes as well[6,8].

To compare phosphorylation occupancy between the Dmanisi and Atapuerca enamel proteomes, we performed a separate MaxQuant database search (Supplementary Information) and restricted our analyses to amino acid positions covered by phosphorylated and non-phosphorylated peptides, observed in both hominins and quantified through label-free quantification.

Phylogenetic analysis

Comparison between the ancient protein sequences and modern reference proteins. We compared the reconstructed ancient protein sequences from the Dmanisi *H. erectus* and Atapuerca *H. antecessor* with protein sequences from great apes[44,46], three Neanderthals[31,43,58], a Denisovan[59] and a panel of present-day humans, including 256 samples from the Simons Genome Diversity Panel[33] and 41 high-coverage individuals from the 1000 Genomes Project[34]. Altogether, our reference data represent worldwide human and great ape variation (Supplementary Tables 7, 8). Additionally, we included protein sequences from macaque (*M. mulatta*) and gibbon (*N. leucogenys*) to root phylogenetic trees. The protein sequences were retrieved from the UniProt database or reconstructed from the reference whole-genome sequences as described in Supplementary Methods.

The ancient and reference protein sequences were aligned using mafft[60]. We aligned the sequences of each protein separately and obtained an alignment for each of the ancient individuals independently (Supplementary Table 9). The isobaric amino acids leucine (L) and isoleucine (I) cannot be distinguished with the experimental procedure used for this study. Therefore, we have to take the following precautions to avoid unintentional sequence differences. If either I or L was present at a specific amino acid position in the reference protein sequences, we replaced all corresponding amino acids in the ancient protein sequences with the amino acid that is present. Alternatively, if both amino acids are present in the reference protein sequence, we replace all I to L for all sequences. We used sequence information for seven proteins (ALB, AMBN, AMELX, AMELY, COL17α1, ENAM and MMP20) for the *H. antecessor* individual and six proteins for the *H. erectus* individual (ALB, AMBN, AMELX, COL17α1, ENAM and MMP20) with a total of 22.08% and 22.14% non-missing sites, respectively (Supplementary Table 9). We were able to recover a unique single amino acid polymorphism for *H. antecessor*; however, for *H. erectus* no unique single amino acid polymorphism was detected (Supplementary Tables 9–11, Supplementary Figs. 10–12).

Phylogenetic reconstruction. We built phylogenetic trees using our protein sequence alignments following three approaches: a maximum likelihood approach using PhyML v.3[61], and two Bayesian approaches using mrBayes[62] and BEAST[63].

For the maximum likelihood approach, we built maximum likelihood trees for each protein independently and for a concatenated alignment consisting of all of the available protein sequences for each of the ancient samples (Supplementary Figs. 13, 14). We used PhyML v.3 and the parameters described in the Supplementary Information section 2.3.5a to build and optimize the tree topologies, branch length and substitutions rates for each of the alignments. Support for each bipartition was obtained based on 100 non-parametric bootstrap replicates. We evaluated the effect of significant missingness in the ancient samples on the inferred topology. Finally, we looked at the effect of varying which of the subset of present-day human samples was included in the tree (Supplementary Information section 2.3.5b, c).

For the Bayesian approach using mrBayes, to assess the robustness of the maximum likelihood inference results, we performed Bayesian phylogenetic inference on the basis of the concatenated alignments using mrBayes 3.2 and the parameters described in Supplementary Information section 2.3.5d (Extended Data Fig. 8, Supplementary Fig. 16). Bayesian inference was performed using the CIPRES Science Gateway[64].

For the Bayesian approach using BEAST, we used BEAST 2.5 to obtain a time calibrated tree for the seven proteins used for *H. antecessor*. For this analysis, we used concatenated alignments including the Neanderthals, the Denisovan, seven randomly chosen *H. sapiens* individuals and a single individual per great ape species. The alignment was partitioned by gene and a coalescent constant population model was used for the tree prior. The dates of the ancient samples included in the analysis (Vindija Neanderthal, 52 ka[58]; Altai Neanderthal, 112 ka[31]; Denisovan, 72 ka[59] and *H. antecessor*, 860.5 ka[11]) were used as tip dates for calibration. For each partition, we used the Jones–Taylor–Thornton substitution model with four categories for the gamma parameter, for which we allowed the Markov chain Monte Carlo chain to sample the shape of the gamma distribution (with an exponentially distributed prior) and assigned independent clock models. Additionally, we set a prior for the divergence time of great apes to 23.85 ± 2.5 Ma (normally distributed)[65], and rooted the tree using the macaque (*M. mulatta*). The overall topology of the tree was estimated for the seven partitions jointly. The convergence of the algorithm was assessed using Tracer v.1.7.0[66]. Finally, we repeated this analysis with 100 alignments, each of them consisting of 7 present-day humans chosen randomly. Although the topology within the clade consisting of present-day humans, Neanderthals and Denisovan was not consistent across the replicates, 99 of the replicates consistently place the *H. antecessor* sequence as an outgroup to this clade (Fig. 2a).

Further details on phylogenetic analysis and results can be found in the Supplementary Information. Example MS/MS spectra from the MaxQuant search and overlapping sites of phylogenetic interest (single amino acid polymorphisms) for both hominins are included as Supplementary Data 1.

Reporting summary

Further information on research design is available in the Nature Research Reporting Summary linked to this paper.

Data availability

Mass spectrometry proteomics data have been deposited in the ProteomeXchange Consortium (http://proteomecentral.proteomexchange.org) via the PRIDE partner repository with the dataset identifier PXD014342. Generated ancient protein consensus sequences used for phylogenetic analysis for *H. antecessor* (Atapuerca) and *H. erectus* (Dmanisi) hominins can be found in the Supplementary Data 2, which is formatted as a .fasta file. Full protein sequence alignments used during phylogenetic analysis can be accessed via Figshare (https://doi.org/10.6084/m9.figshare.9927074). Amino acid racemization data are available online through the NOAA database. The wiNNer model can be accessed on GitHub (https://github.com/cox-labs/wiNNer.git).

39. Penkman, K. E. H., Kaufman, D. S., Maddy, D. & Collins, M. J. Closed-system behaviour of the intra-crystalline fraction of amino acids in mollusc shells. *Quat. Geochronol.* **3**, 2–25 (2008).
40. Dickinson, M., Lister, A. M. & Penkman, K. E. H. A new method for enamel amino acid racemization dating: a closed system approach. *Quat. Geochronol.* **50**, 29–46 (2019).
41. Hill, R. L. Hydrolysis of proteins. *Adv. Protein Chem.* **20**, 37–107 (1965).
42. Mackie, M. et al. Palaeoproteomic profiling of conservation layers on a 14th century italian wall painting. *Angew. Chem. Int. Ed. Engl.* **57**, 7369–7374 (2018).
43. Castellano, S. et al. Patterns of coding variation in the complete exomes of three Neandertals. *Proc. Natl Acad. Sci. USA* **111**, 6666–6671 (2014).
44. de Manuel, M. et al. Chimpanzee genomic diversity reveals ancient admixture with bonobos. *Science* **354**, 477–481 (2016).
45. Nater, A. et al. Morphometric, behavioral, and genomic evidence for a new orangutan species. *Curr. Biol.* **27**, 3487–3498.e10 (2017).
46. Prado-Martinez, J. et al. Great ape genetic diversity and population history. *Nature* **499**, 471–475 (2013).

47. Hanson-Smith, V. & Johnson, A. PhyloBot: a web portal for automated phylogenetics, ancestral sequence reconstruction, and exploration of mutational trajectories. *PLOS Comput. Biol.* **12**, e1004976 (2016).
48. Welker, F. Elucidation of cross-species proteomic effects in human and hominin bone proteome identification through a bioinformatics experiment. *BMC Evol. Biol.* **18**, 23 (2018).
49. Hendy, J. et al. A guide to ancient protein studies. *Nat. Ecol. Evol.* **2**, 791–799 (2018).
50. Zhang, J. et al. PEAKS DB: de novo sequencing assisted database search for sensitive and accurate peptide identification. *Mol. Cell. Proteomics* **11**, M111.010587 (2012).
51. Cox, J. & Mann, M. MaxQuant enables high peptide identification rates, individualized p.p.b.-range mass accuracies and proteome-wide protein quantification. *Nat. Biotechnol.* **26**, 1367–1372 (2008).
52. Chun, Y. H. P. et al. Cleavage site specificity of MMP-20 for secretory-stage ameloblastin. *J. Dent. Res.* **89**, 785–790 (2010).
53. Yamakoshi, Y., Hu, J. C. C., Fukae, M., Yamakoshi, F. & Simmer, J. P. How do enamelysin and kallikrein 4 process the 32-kDa enamelin? *Eur. J. Oral Sci.* **114** (Suppl 1), 45–51, 93–95, 379–380 (2006).
54. Iwata, T. et al. Processing of ameloblastin by MMP-20. *J. Dent. Res.* **86**, 153–157 (2007).
55. Nagano, T. et al. Mmp-20 and Klk4 cleavage site preferences for amelogenin sequences. *J. Dent. Res.* **88**, 823–828 (2009).
56. Fukae, M. et al. Primary structure of the porcine 89-kDa enamelin. *Adv. Dent. Res.* **10**, 111–118 (1996).
57. Colaert, N., Helsens, K., Martens, L., Vandekerckhove, J. & Gevaert, K. Improved visualization of protein consensus sequences by iceLogo. *Nat. Methods* **6**, 786–787 (2009).
58. Prüfer, K. et al. A high-coverage Neandertal genome from Vindija Cave in Croatia. *Science* **358**, 655–658 (2017).
59. Meyer, M. et al. A high-coverage genome sequence from an archaic Denisovan individual. *Science* **338**, 222–226 (2012).
60. Katoh, K., Misawa, K., Kuma, K. & Miyata, T. MAFFT: a novel method for rapid multiple sequence alignment based on fast Fourier transform. *Nucleic Acids Res.* **30**, 3059–3066 (2002).
61. Guindon, S. et al. New algorithms and methods to estimate maximum-likelihood phylogenies: assessing the performance of PhyML 3.0. *Syst. Biol.* **59**, 307–321 (2010).
62. Ronquist, F. et al. MrBayes 3.2: efficient Bayesian phylogenetic inference and model choice across a large model space. *Syst. Biol.* **61**, 539–542 (2012).
63. Bouckaert, R. et al. BEAST 2.5: An advanced software platform for Bayesian evolutionary analysis. *PLOS Comput. Biol.* **15**, e1006650 (2019).
64. Miller, M. A., Pfeiffer, W. & Schwartz, T. in *Gateway Computing Environments Workshop (GCE)* 1–8 (New Orleans, 2010).
65. Besenbacher, S., Hvilsom, C., Marques-Bonet, T., Mailund, T. & Schierup, M. H. Direct estimation of mutations in great apes reconciles phylogenetic dating. *Nat. Ecol. Evol.* **3**, 286–292 (2019).
66. Rambaut, A., Drummond, A. J., Xie, D., Baele, G. & Suchard, M. A. Posterior summarization in Bayesian phylogenetics using Tracer 1.7. *Syst. Biol.* **67**, 901–904 (2018).

Acknowledgements F.W. is supported by a Marie Skłodowska Curie Individual Fellowship (no. 795569). E. Cappellini was supported by VILLUM FONDEN (no. 17649). E.W. is supported by the Lundbeck Foundation, the Danish National Research Foundation, the Novo Nordisk Foundation, the Carlsberg Foundation, KU2016 and the Wellcome Trust. Without the effort of the members of the Atapuerca research team during fieldwork, this work would have not been possible; we make a special mention of J. Rosell, who supervises the excavation of the TD6 level. The research of the Atapuerca project has been supported by the Dirección General de Investigación of the Ministerio de Ciencia, Innovación y Universidades (grant numbers PGC2018-093925-B-C31, C32, and C33); field seasons are supported by the Consejería de Cultura y Turismo of the Junta de Castilla y León and the Fundación Atapuerca. We acknowledge The Leakey Foundation through the personal support of G. Getty (2013) and D. Crook (2014–2016, 2018, and 2019) to M.M.-T., as well as F.W. (2017). Restoration and conservation work on the material have been carried out by P. Fernández-Colón and E. Lacasa from the Conservation and Restoration Area of CENIEH-ICTS and L. López-Polín from IPHES. The picture of the specimen ATD6-92 was made by M. Modesto-Mata. E. Cappellini, J.C., J.V.O. and P. Gutenbrunner are supported by the Marie Skłodowska-Curie European Training Network (ETN) TEMPERA, a project funded by the European Union's Framework Program for Research and Innovation Horizon 2020 (grant agreement no. 722606). Amino acid analyses were undertaken thanks to the Leverhulme Trust (PLP-2012-116) and NERC (NE/K500987/1). T.M.-B. is supported by BFU2017-86471-P (MINECO/FEDER, UE), U01 MH106874 grant, Howard Hughes International Early Career, Obra Social 'La Caixa' and Secretaria d'Universitats i Recerca and CERCA Programme del Departament d'Economia i Coneixement de la Generalitat de Catalunya (GRC 2017 SGR 880). C.L.-F. is supported by a FEDER-MINECO grant (PGC2018-095931-B-100). M.K. was supported by the Postdoctoral Junior Leader Fellowship Programme from 'la Caixa' Banking Foundation (LCF/BQ/PR19/11700002). M.M. is supported by the Danish National Research Foundation award PROTEIOS (DNRF128). Work at the Novo Nordisk Foundation Center for Protein Research is funded in part by a donation from the Novo Nordisk Foundation (grant number NNF14CC0001). The CRG/UPF Proteomics Unit is part of the Spanish Infrastructure for Omics Technologies (ICTS OmicsTech) and it is a member of the ProteoRed PRB3 consortium, which is supported by grant PT17/0019 of the PE I+D+i 2013-2016 from the Instituto de Salud Carlos III (ISCIII) and ERDF. We acknowledge support from the Spanish Ministry of Science, Innovation and Universities, 'Centro de Excelencia Severo Ochoa 2013-2017', SEV-2012-0208, and 'Secretaria d'Universitats i Recerca del Departament d'Economia i Coneixement de la Generalitat de Catalunya' (2017SGR595). D.L. and A.M. are supported by the John Templeton Foundation (no. 52935) and by the Shota Rustaveli National Science Foundation of Georgia (no. FR-18-27262). We thank M. L. Schjellerup Jørkov for providing specimen Ø1952.

Author contributions E. Cappellini, E.W., J.M.B.d.C., D.L., C.L.-F. and F.W. designed the study. E. Cappellini, M.M., F.W., J.R.-M., R.R.J.-C., M.R.D., C.C. and M.d.M. performed experiments. E. Cappellini, A.M., J.L.A., E. Carbonell, P. Gelabert, E.S., J.C., J.V.O., T.M.-B. and D.L. provided material, reagents or research infrastructure. F.W., J.R.-M., P. Gutenbrunner, S.T., E. Cappellini, F.R., M.M.-T., J.M.B.d.C., M.K., M.R.D., C.L.-F. and K.P. analysed data. F.W., E. Cappellini and J.M.B.d.C. wrote the manuscript with input from all other authors.

Competing interests The authors declare no competing interests.

Additional information

Supplementary information is available for this paper at https://doi.org/10.1038/s41586-020-2153-8.

Correspondence and requests for materials should be addressed to F.W., J.M.B.d.C., E.W. or E.C.

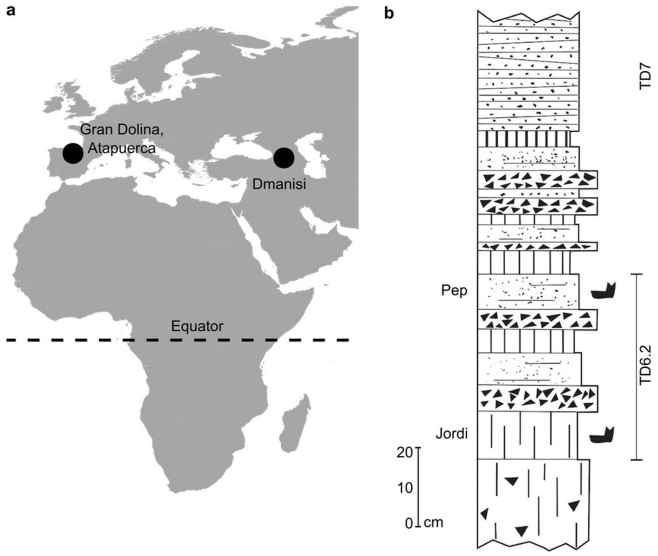

Extended Data Fig. 1 | Location and stratigraphy of the hominin fossils studied. a, Geographic location of Gran Dolina and Dmanisi. Base map was generated using public domain data from www.naturalearthdata.com. **b**, Summarized stratigraphic profile of Gran Dolina, including the location of hominin fossils in layers 'Pep' and 'Jordi' of sublevel TD6.2.

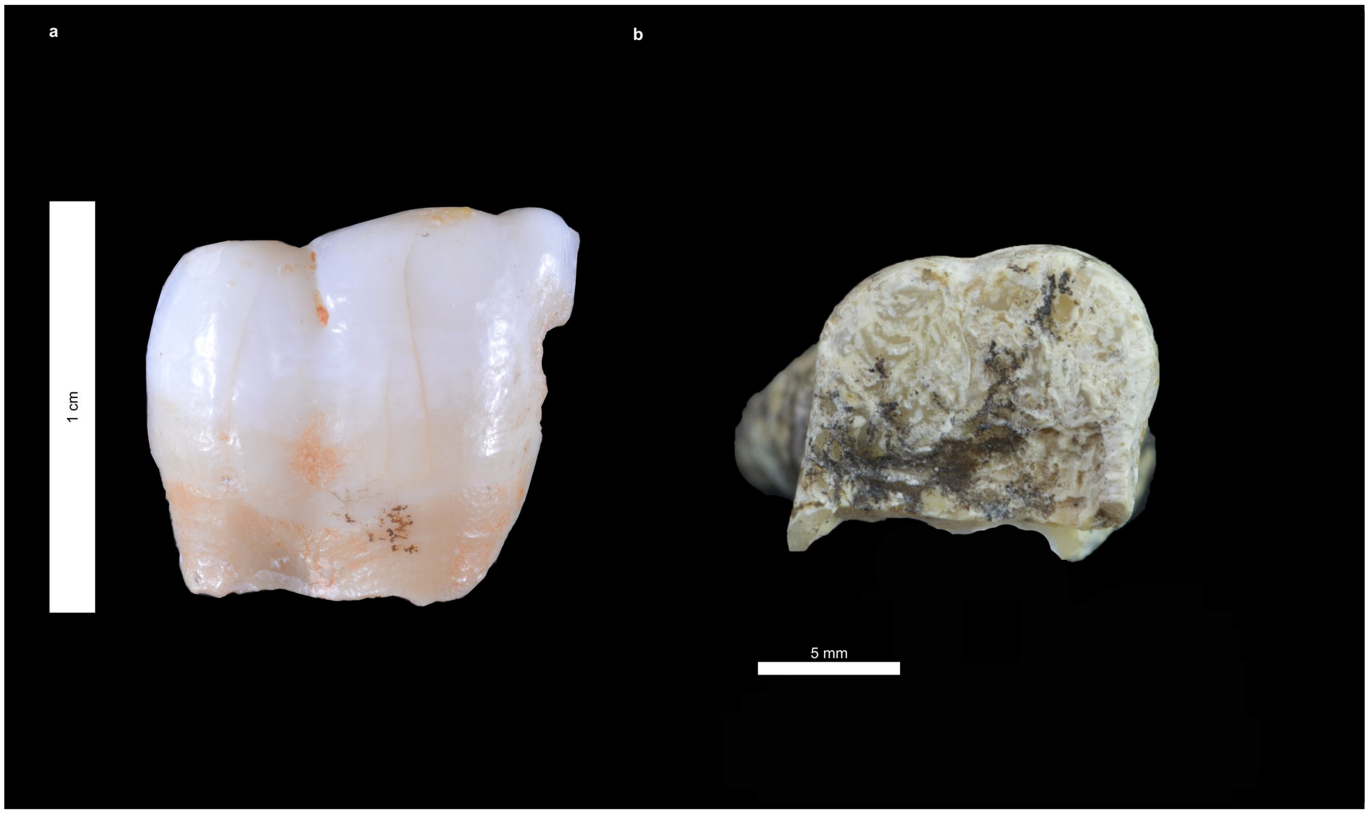

Extended Data Fig. 2 | Hominin specimens studied. a, ATD6-92 in buccal view. The fragment represents a portion of a permanent lower left first or second molar. **b**, D4163 in occlusal view. The specimen is a fragmented right upper first molar. Scale bar differs between **a** and **b**.

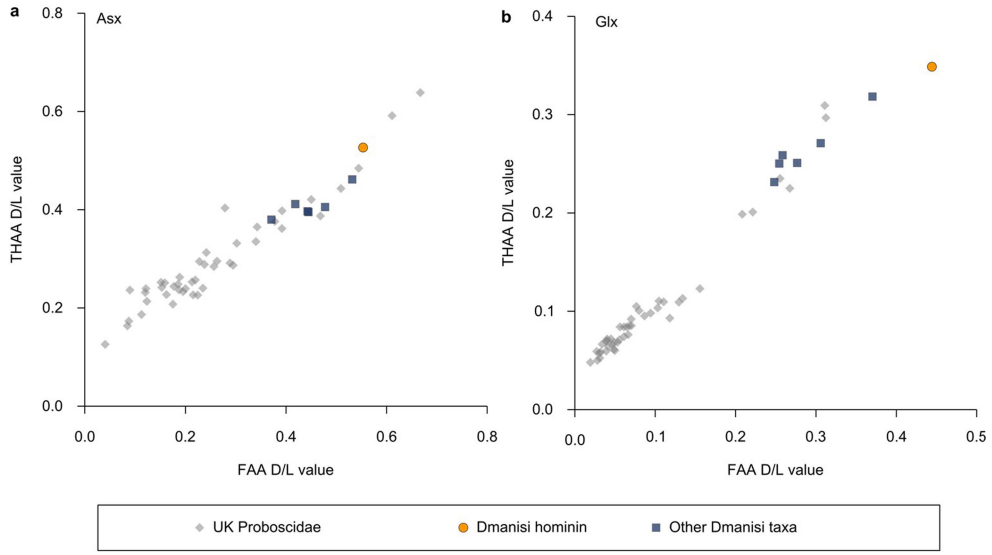

Extended Data Fig. 3 | Amino acid racemization of D4163. a, **b**, The extent of intracrystalline racemization in enamel for the free amino acid (FAA) (*x* axis) fraction and the total hydrolysable amino acids (THAA) (*y* axis) fraction for aspartic acid plus asparagine (here denoted Asx) (**a**), and glutamic acid plus glutamine (here denoted Glx) (**b**), demonstrates endogenous amino acids breaking down within a closed system. The hominin value is displayed in relation to values for enamel samples from other fauna from Dmanisi[6] (blue squares) and a range of previously obtained Pleistocene and Pliocene Proboscidea from the UK[40] (grey diamonds). Fauna are shown for comparison, but different rates in their protein breakdown mean that they will show different extents of racemization. The *x* and *y* axis are on different scales.

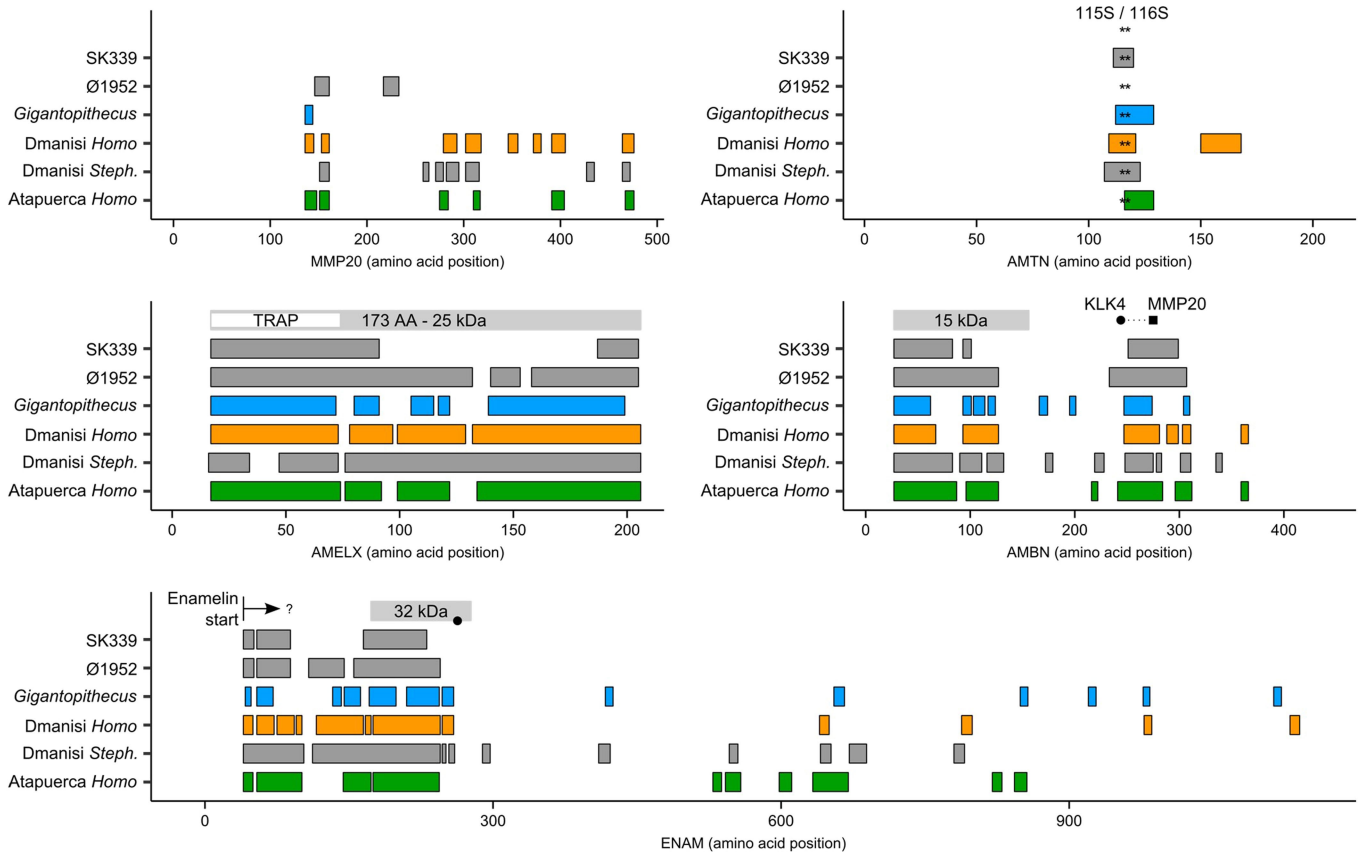

Extended Data Fig. 4 | Sequence coverage for five enamel-specific proteins across Pleistocene samples and recent human controls. For each protein, the bars span protein positions covered, with positions remapped to the human reference proteome. The top row indicates the position of a selection of known MMP20 and KLK4 cleavage products of the enamel-specific proteins AMELX[55], AMBN[52] and ENAM[56]. Several in vivo proteolytic degradation fragments of ENAM share the same N terminus, but have unknown C termini[53]. Dotted line for AMBN indicates a putative cleavage product based on known MMP20 (squares) and KLK4 (circles) in vivo cleavage positions. For AMTN, serines (S) at positions 115 and 116 (indicated by asterisks) are conserved among vertebrates and involved in mineral-binding[21]. Additional cleavage products as well as MMP20 and KLK4 cleavage sites are known in all enamel-specific proteins. SK339[16] and Ø1952 are two recent human control samples (Methods). AA, amino acids; *Steph.*, *Stephanorhinus*[6]; TRAP, tyrosine-rich amelogenin polypeptide.

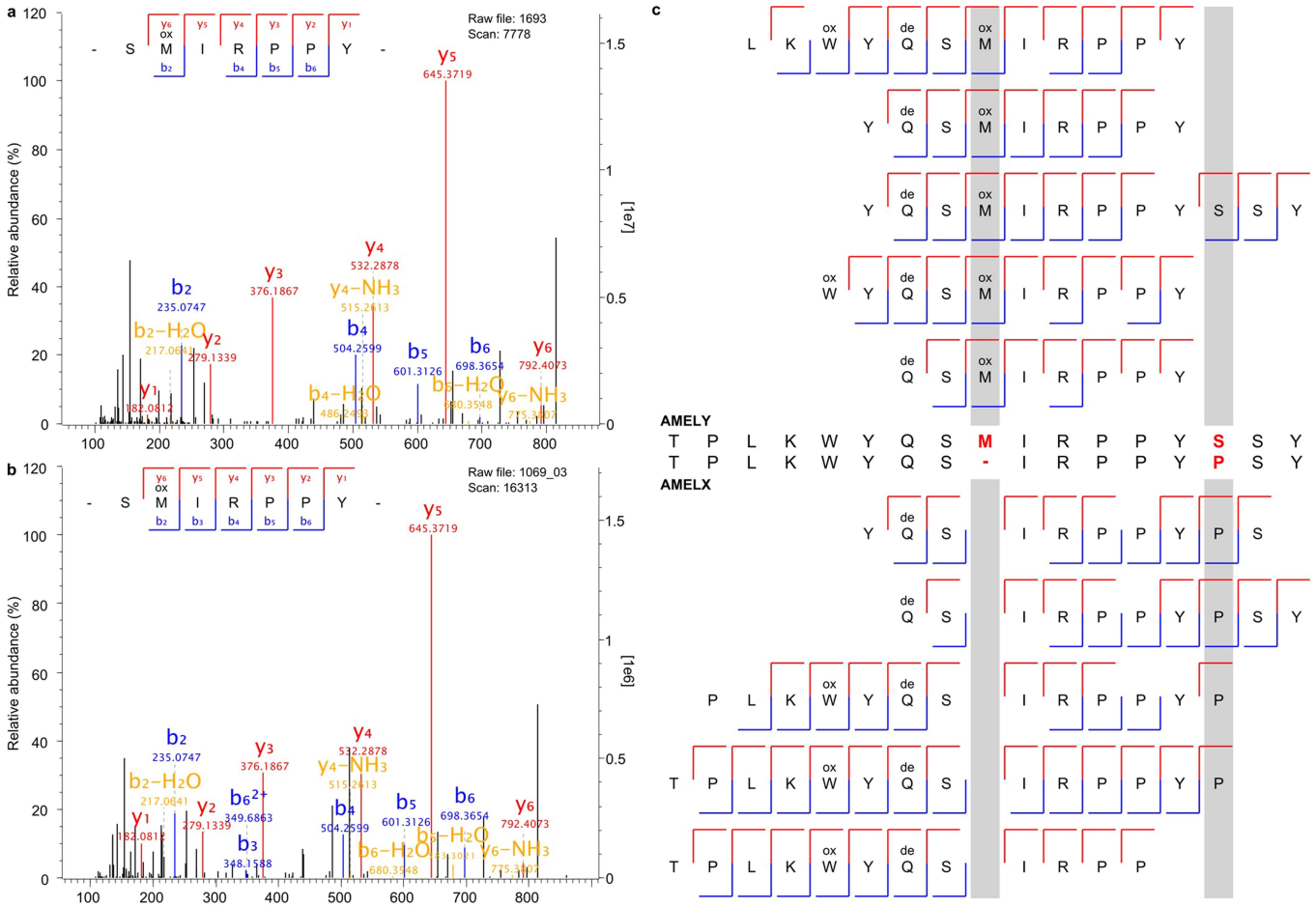

Extended Data Fig. 5 | *Homo antecessor* specimen ATD6-92 represents a male hominin. a, Mass spectrum of an AMELY-specific peptide from the recent human control Ø1952. **b**, Mass spectrum of the same AMELY-specific peptide from *H. antecessor*. **c**, Alignment of a selection of AMELY- and AMELX-specific peptide fragment ion series deriving from *H. antecessor*. The alignment stretches along human AMELX isoform 1, positions 37 to 52 only (Uniprot accession numbers Q99217 (AMELX), Q99218 (AMELY)). See Supplementary Fig. 5 for another example of an AMELY-specific MS2 spectrum.

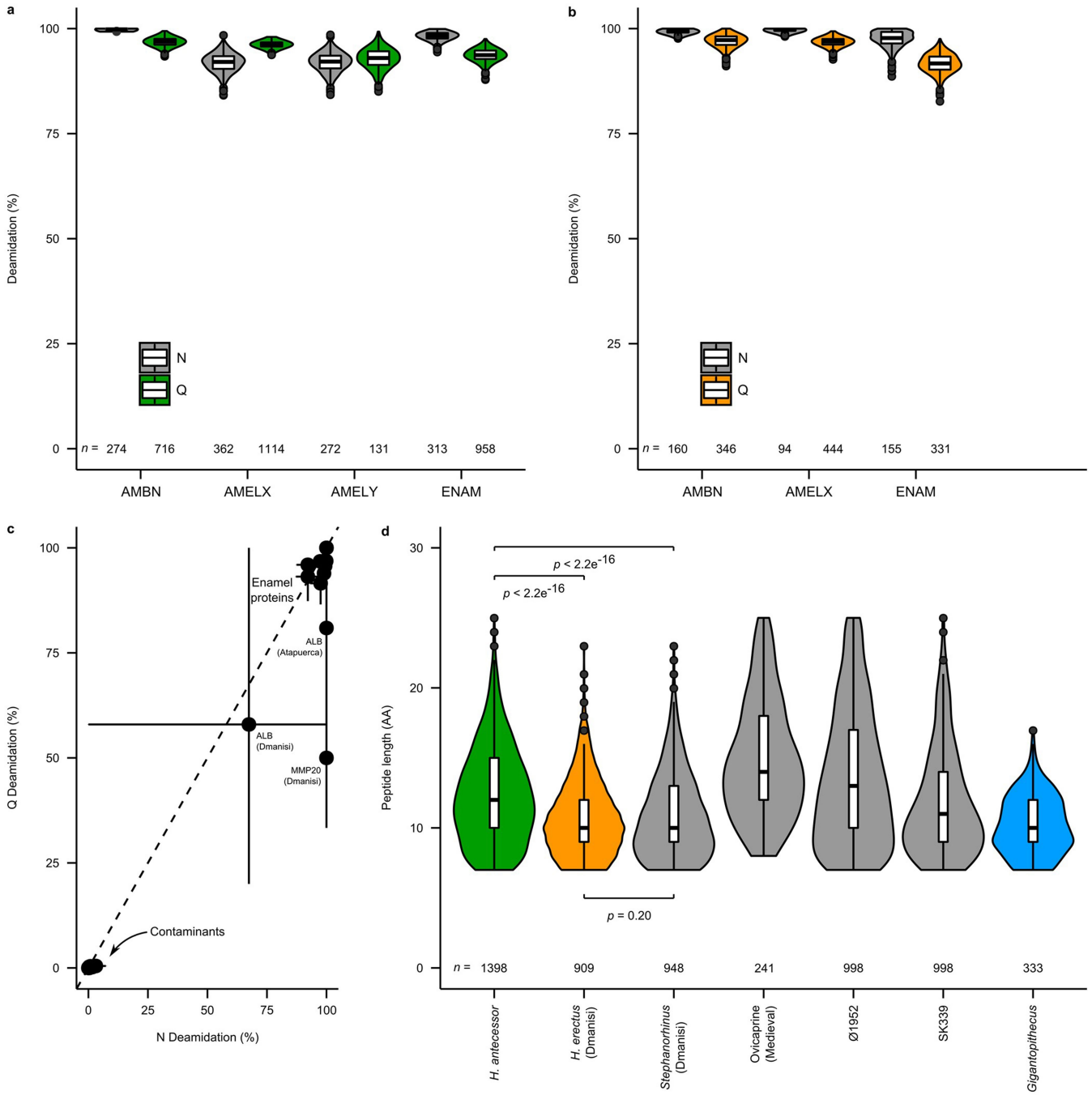

Extended Data Fig. 6 | Enamel proteome damage. a, **b**, Glutamine (Q) and asparagine (N) deamidation of enamel-specific proteins from *H. antecessor* (Atapuerca) (**a**), and *H. erectus* (Dmanisi) (**b**). Values are based on 1,000 bootstrap replications of protein deamidation. **c**, Relationship between mean asparagine (N) and glutamine (Q) deamidation for all proteins in both the Atapuerca and Dmanisi hominin datasets. Error bars represent 95% confidence interval window of 1,000 bootstrap replications of protein deamidation. Dashed line is $x = y$. **d**, Peptide length distribution of *H. antecessor* (Atapuerca), *H. erectus* (Dmanisi), four previously published enamel proteomes[6,8,16] and one additional human Medieval control sample (Ø1952). For **a**, **b** and **d**, the number of peptides (*n*) is given for each violin plot. The box plots within the violin plots define the range of the data (whiskers extend to 1.5× the interquartile range), outliers (black dots, beyond 1.5× the interquartile range), 25th and 75th percentiles (boxes), and medians (centre lines). *P* values of two-sided *t*-tests conducted between sample pairs are indicated. No independent replication of these experiments was performed.

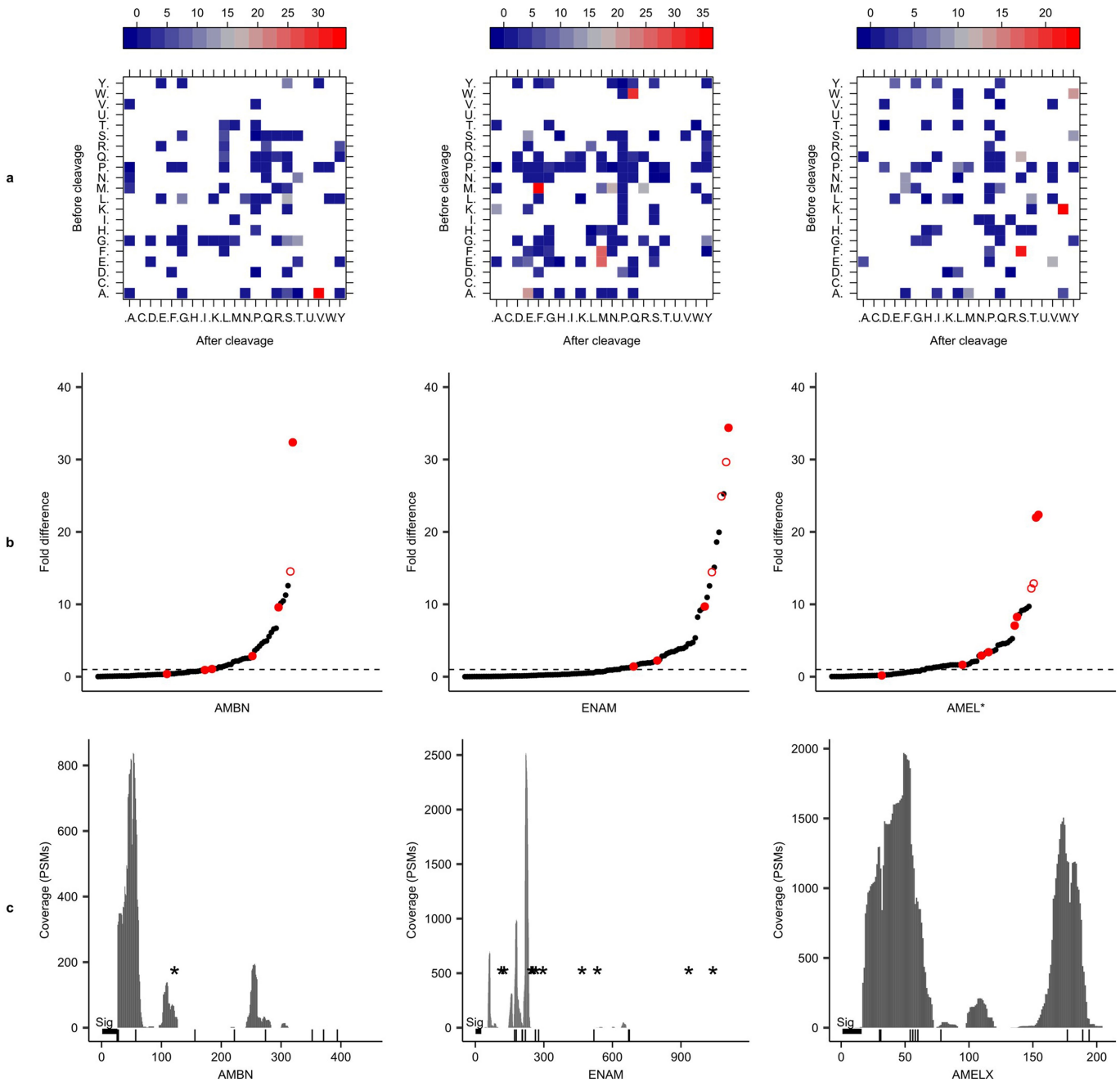

Extended Data Fig. 7 | Survival of in vivo MMP20 and KLK4 cleavage sites in the Atapuerca enamel proteome. a, Experimentally observed cleavage matrices for ameloblastin (AMBN), enamelin (ENAM) and amelogenin (AMELX and AMELY) (Methods). Fold differences are colour-coded by comparing observed PSM cleavage frequencies to a random cleavage matrix for each protein separately[7]. **b**, Fold differences for all observed cleavage pairs per protein. Red filled circles represent MMP20, KLK4 and signal peptide cleavage sites mentioned in the literature[53–56]. Red open circles indicate cleavage sites located up to two amino acid positions away from such sites. **c**, PSM coverage for each protein. The signal peptide (thick horizontal bar labelled 'sig'), known MMP20 and KLK4 cleavage sites (vertical bars), and O- and N-linked glycosylation sites (asterisks) are also indicated. For AMELX, peptide positions for all three known isoforms were remapped to the coordinates of isoform 3, which represents the longest isoform (UniProt accession Q99217-3). The *x* and *y* axes differ between the three panels of **c**.

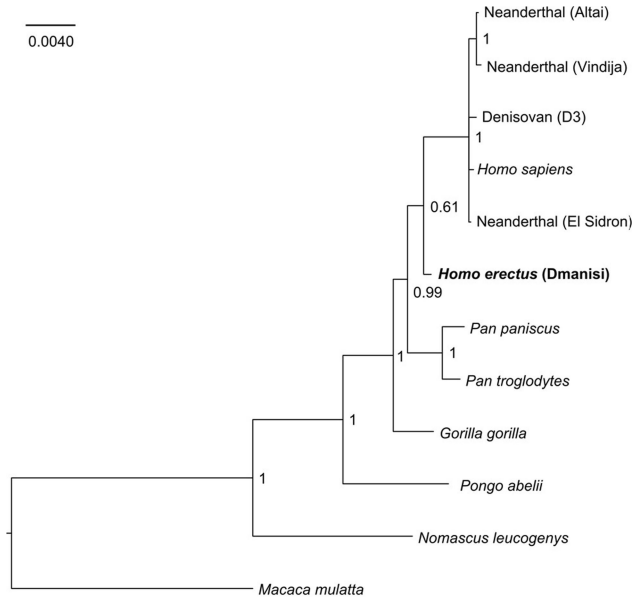

Extended Data Fig. 8 | Phylogenetic position of D4163 through Bayesian analysis. *Nomascus leucogenys* and *M. mulatta* were used as outgroups.

Extended Data Table 1 | Extraction and mass spectrometry details of analyses conducted on both ancient hominin specimens

Stage Tip number	Tissue	Protein extraction method*	Mass Spectrometer	Mass Spectrometer location	Replicates
***Homo antecessor*, specimen ATD6-92, Atapuerca**					
1069	Enamel	1	QE-HF	Copenhagen	4
1069	Enamel	1	Fusion Lumos	Barcelona	1
***Homo erectus*, specimen D4163, Dmanisi**					
1138	Enamel	1	QE-HF	Copenhagen	2
1141	Enamel	2	QE-HF	Copenhagen	2
1138	Enamel	1	Fusion Lumos	Barcelona	1
1141	Enamel	2	Fusion Lumos	Barcelona	1
1139	Dentine	1	QE-HF	Copenhagen	2
1142	Dentine	2	QE-HF	Copenhagen	2
1139	Dentine	1	Fusion Lumos	Barcelona	1
1142	Dentine	2	Fusion Lumos	Barcelona	1
1386	Enamel	1	QE-HF	Copenhagen	1
1387	Enamel	3	QE-HF	Copenhagen	1
1388	Enamel	1	QE-HF	Copenhagen	1

QE-HF, Q Exactive HF (or HF-X) hybrid quadrupole-Orbitrap mass spectrometer (Thermo Fisher Scientific). Fusion Lumos, LTQ-Orbitrap Fusion Lumos mass spectrometer (Thermo Fisher Scientific).
*Extraction method 1: demineralization in HCl, with no subsequent proteolytic digestion. Extraction method 2: demineralization in HCl, reduction, alkylation and digestion with LysC and trypsin. Extraction method 3: demineralization in TFA, with no subsequent proteolytic digestion. See Supplementary Information for further details.

Extended Data Table 2 | Ancient hominin enamel proteome composition and coverage

Protein	Primary accession	MaxQuant Peptides	MaxQuant Unique peptides	MaxQuant Coverage (AA)	MaxQuant Coverage (%)	PEAKS Peptides	PEAKS Unique peptides	PEAKS Coverage (AA)	PEAKS Coverage (%)	Combined Coverage (%)
***Homo antecessor*, specimen ATD6-92, Atapuerca**										
AMELX	Q99217*	527	527	170 (0)	82.9	737	12	171 (1)	83.4	83.4
AMELY	Q99218*	220	86	131 (0)	63.6	341	6	141 (10)	68.4	68.4
AMBN	Q9NP70*	289	289	160 (3)	35.8	351	350	166 (9)	37.1	37.8
AMTN	Q6UX39	4	4	14	6.7	5	5	14	6.7	6.7
ENAM	Q9NRM1	424	424	233 (18)	20.4	586	586	245 (32)	21.5	23.0
MMP20	O60882	12	12	65 (0)	13.5	14	14	66 (1)	13.7	13.7
ALB	P02768	11	11	69 (17)	11.3	12	7	76 (24)	12.5	15.3
COL1α1	P02452	17	17	34 (21)	2.3	15	15	29 (16)	2.0	3.4
COL1α2	P08123	1	1	23	1.7	2	2	23	1.7	1.7
COL17α1	Q9UMD9	27	27	96 (24)	6.4	42	42	88 (16)	5.9	7.5
***Homo erectus*, specimen D4163, Dmanisi**										
AMELX	Q99217*	357	357	182 (9)	88.8	297	297	173 (0)	84.4	88.8
AMBN	Q9NP70*	219	219	123 (1)	27.5	182	182	139 (17)	31.1	31.3
AMTN	Q6UX39	6	6	31 (13)	15.3	1	1	18 (0)	9.1	14.8
ENAM	Q9NRM1	306	306	224 (78)	19.6	293	293	160 (14)	14.0	20.8
MMP20	O60882	13	13	90 (15)	18.6	16	16	84 (9)	17.4	20.5
ALB	P02768	33	33	216 (12)	35.5	41	28	233 (29)	38.3	40.2
COL1α1	P02452	10	10	202 (44)	13.8	17	17	414 (256)	28.3	31.3
COL1α2	P08123	9	9	130 (3)	9.5	11	11	197 (66)	14.6	14.6
COL17α1	Q9UMD9	10	10	67 (45)	4.5	1	1	22 (0)	1.5	4.5

Proteins are included only if two or more unique peptides were observed in either the PEAKS or MaxQuant searches. Primary accession refers to the *H. sapiens* entry in UniProt. Protein sequence coverage in the final column indicates the coverage obtained after combining PEAKS and MaxQuant peptide recovery. For 'coverage (AA)' columns, numbers in parentheses refer to the number of amino acid (AA) positions uniquely identified in PEAKS or MaxQuant searches. For AMELX and AMELY, coverage statistics combine counts for all isoforms present, whereas peptide counts refer only to the highest-ranking isoform or database entry. Direct comparisons between PEAKS and MaxQuant are uninformative owing to fundamental differences in spectral identification, protein and/or peptide assignment, and peptide counting approaches.

*Combined coverage calculated against the longest isoforms for each protein.

Corresponding author(s): Enrico Cappellini
Eske Willerlev
Jose-Maria Bermudez de Castro
Frido Welker

Reporting Summary

Nature Research wishes to improve the reproducibility of the work that we publish. This form provides structure for consistency and transparency in reporting. For further information on Nature Research policies, see Authors & Referees and the Editorial Policy Checklist.

Statistical parameters

When statistical analyses are reported, confirm that the following items are present in the relevant location (e.g. figure legend, table legend, main text, or Methods section).

n/a	Confirmed
☐	☒ The exact sample size (*n*) for each experimental group/condition, given as a discrete number and unit of measurement
☐	☒ An indication of whether measurements were taken from distinct samples or whether the same sample was measured repeatedly
☐	☒ The statistical test(s) used AND whether they are one- or two-sided *Only common tests should be described solely by name; describe more complex techniques in the Methods section.*
☒	☐ A description of all covariates tested
☒	☐ A description of any assumptions or corrections, such as tests of normality and adjustment for multiple comparisons
☐	☒ A full description of the statistics including central tendency (e.g. means) or other basic estimates (e.g. regression coefficient) AND variation (e.g. standard deviation) or associated estimates of uncertainty (e.g. confidence intervals)
☐	☒ For null hypothesis testing, the test statistic (e.g. *F*, *t*, *r*) with confidence intervals, effect sizes, degrees of freedom and *P* value noted *Give P values as exact values whenever suitable.*
☐	☒ For Bayesian analysis, information on the choice of priors and Markov chain Monte Carlo settings
☒	☐ For hierarchical and complex designs, identification of the appropriate level for tests and full reporting of outcomes
☒	☐ Estimates of effect sizes (e.g. Cohen's *d*, Pearson's *r*), indicating how they were calculated
☐	☒ Clearly defined error bars *State explicitly what error bars represent (e.g. SD, SE, CI)*

Our web collection on statistics for biologists may be useful.

Software and code

Policy information about availability of computer code

Data collection	Mass spectrometric data were acquired using the Xcalibur™ Software, controlling the Thermo Scientific™ LC-MS systems.
Data analysis	Xcalibur™ (version 4.1) MaxQuant (version 1.5.3.30) PEAKS (version 7.5) Geneious (version 5.4.4) Python (version 3.5.4) Keras (version 2.0.8) Tensorflow (version 1.3.0) samtools (version 0.1.18) ANGSD (version 0.913) mafft (version 7.205) Phangorn (version 2.4.0, R version 3.4.2) BWA-MEM (version 0.7.7) PICARD (version 1.91) GATK UnifiedGenotyper (version 3.4-46) blastall (version 2.2.26) PHyML (version 3.1)

MrBayes (version 3.2.6)
R (version 3.4.3)
R, package vioplot (version 0.2)
R, package ggplot2 (version 3.1.0 and version 3.1.1)
R, package stringr (version 1.4.0)
R, package stringi (version 1.2.4)
Tracer (version 1.7.0)
BEAST (version 2.5)
https://github.com/cox-labs/wiNNer.git

For manuscripts utilizing custom algorithms or software that are central to the research but not yet described in published literature, software must be made available to editors/reviewers upon request. We strongly encourage code deposition in a community repository (e.g. GitHub). See the Nature Research guidelines for submitting code & software for further information.

Data

Policy information about availability of data

All manuscripts must include a data availability statement. This statement should provide the following information, where applicable:

- Accession codes, unique identifiers, or web links for publicly available datasets
- A list of figures that have associated raw data
- A description of any restrictions on data availability

All the mass spectrometry proteomics data have been deposited in the ProteomeXchange Consortium (http://proteomecentral.proteomexchange.org) via the PRIDE partner repository with the data set identifier PXD014342 Protein sequences generated as part of this study are provided as supplementary files.

Field-specific reporting

Please select the best fit for your research. If you are not sure, read the appropriate sections before making your selection.

☒ Life sciences ☐ Behavioural & social sciences ☐ Ecological, evolutionary & environmental sciences

For a reference copy of the document with all sections, see nature.com/authors/policies/ReportingSummary-flat.pdf

Life sciences study design

All studies must disclose on these points even when the disclosure is negative.

Sample size	No sample size calculation was required. All available hominin specimens available to us (n=2) were analyzed, one from each hominin population of interest (Homo antecessor and Homo erectus).
Data exclusions	No data was excluded from the study.
Replication	Phylogenetic trees were reproduced using three different algorithms, and found consistent results (see Methods and SI). Proteomic results were replicated using repeated LC-MS/MS runs of different extracts for enamel of the same teeth, sometimes based on alternative extraction protocols, with extractions performed on different days in different laboratory sessions. Protein extracts were analyzed by LC-MS/MS on separate instruments in Copenhagen and Barcelona, with similar results obtained.
Randomization	Samples were injected in the LC-MS/MS system in randomised order.
Blinding	Blinding was not relevant to this study, with only two specimens analyzed

Reporting for specific materials, systems and methods

Materials & experimental systems

n/a	Involved in the study
☒	☐ Unique biological materials
☒	☐ Antibodies
☒	☐ Eukaryotic cell lines
☐	☒ Palaeontology
☒	☐ Animals and other organisms
☒	☐ Human research participants

Methods

n/a	Involved in the study
☒	☐ ChIP-seq
☒	☐ Flow cytometry
☒	☐ MRI-based neuroimaging

Palaeontology

Specimen provenance	Studied specimens derive from Gran Dolina, Atapuerca (Spain) and Dmanisi (Georgia). Export of specimens to the Globe Institute, University of Copenhagen was regulated by approval of Prof. J.M Bermudez de Castro (Atapuerca) and Prof. D. Lordkipanidze (Dmanisi) who are both co-authors of the current study.
Specimen deposition	Specimens are available upon request to E. Cappellini (Globe Institute, University of Copenhagen, Denmark), Prof. Bermudez de Castro (CENIEH, Burgos, Spain), or Prof. Lordkipanidze (Georgian National Museum, Georgia).
Dating methods	No new dates obtained.

☐ Tick this box to confirm that the raw and calibrated dates are available in the paper or in Supplementary Information.